Supporting information for:

A Permeability-limited Physiologically Based Pharmacokinetic (PBPK) Model for Perfluorooctanoic acid (PFOA) in Male Rats

Weixiao Cheng and Carla A. Ng*

Department of Civil and Environmental Engineering, University of Pittsburgh, Pittsburgh, Pennsylvania 15261, USA

There are 23 pages, 6 figures and 8 tables included in the supporting information.

Table of Contents

S1 Rat Physiology.

Table S1. Male rat physiological parameters.

	Blood	Liver	Kidney	Gut	Muscle	Adipose	Rest of Body
Fractional Volume (%BW)	5.4[1 a]	3.66[2]	0.73[2]	2.69[2]	40.43[2]	7[2]	40.09[b]
Blood Flow Rate[2 c] (%)	-	2.4	14.1	15.1	27.8	7	33.6[b]
Interstitial Fluid (mL/g tissue)	-	0.049[3]	0.13[4]	0.28[5]	0.054[6]	0.174[6]	0.18[d]
Blood Volume (mL/g tissue)	-	0.21[2]	0.16[2]	0.034[7]	0.04[2]	0.02[2]	0.036[e]
Capillary Surface Area[8 f] (cm^2/g)	-	250	350	100	70	70	100
Bile Duct Volume[3]	0.4% liver tissue volume						
Renal Filtrate Volume[g]	0.25 mL						
Gut Lumen Volume[9]	4.5% BW						
Glomerular Filtration Rate[10]	10.74 mL/min/kg BW						
Urine Flow Rate[1]	200 mL/d/kg BW						
Bile Flow Rate[1]	90 mL/d/kg BW						
Feces Flow Rate[h]	5.63 mL water per day						

Volume calculations were based on density of 1 g/mL^2.

[a] Plasma volume is 3.12 % of body weight (BW)[1].

[b] Fractional volume and blood flow rate were calculated by subtracting the fraction of other tissues from 1.

[c] Expressed as the percent of cardiac output (Q_c); $Q_c = 0.235 \times BW^{0.75}$ L/min, where the unit of BW is kg.

[d] Based on data availability, it was assumed to be the weighted average of brain, heart and spleen fluids[11].

[e] Calculated on the weighted average of blood volume of the "rest of body"[2].

[f] Only the data for liver, kidney and muscle were available, the capillary surface area of other tissues was assumed; in kidney, the surface area of glomerular capillary, through which blood filters into filtrate compartment, is 6890 mm^2/g kidney[12]. Moreover, the area for exchange between each subcompartment was assumed to be the same as the capillary surface area of each tissue, except for the apical membrane of enterocytes and proximal tubules. The microvilli located on these two apical membranes could increase the corresponding surface area significantly. Taking this into consideration, the surface area of gut lumen would be 4.14 m^2/kg BW[13]; and the area of apical membrane of proximal tubule would be increased by a factor of 5, which was assumed the same as the enlargement factor used in describing area increasing due to the numerous projections formed on intestinal wall[13].

[g] To calculate the volume of filtrate compartment, we considered the tubular lumen as a cylinder with length of 5.16 mm[14] and diameter of 45 μm[15], and there are about 30000 nephrons in adult rats[16], therefore, the volume of the filtrate compartment for an adult rat was estimated to be 0.25 mL.

[h] We assumed the PFOA was associated with the water content of feces, which was estimated to be 45% of total fecal weight[17]. Additionally, we used an estimate of fecal production for male Sprague–Dawley rats of 6.88 g dry weight per day[18]. Given these data the fecal water content was determined.

S2 Protein-related Parameters.

S2-1. Protein concentration.

The *in-vitro* studies measured uptake kinetics of PFOA into cells in units of nmol/mg protein/min (normalized to the total protein content in the cells). The total protein content of each tissue (Table S2) was used in our model to convert the *in vitro* uptake value to a first-order rate constant for transport (in units of s^{-1}) specific to each type of tissue.

Table S2. Protein concentration in compartments.

	C_{total} [19 a] (mg/mL)	C_{Alb} (µmol/L)	$C_{L\text{-}FABP}$ (µmol/L)	$C_{\alpha 2u\text{-}globulin}$ (µmol/L)[e]
Plasma	67	486[1 b]		
Liver Fluid		243[20]		
Liver Tissue	40		133[21 d]	
Kidney Fluid		243[c]		
Kidney Tissue	34		2.65[22]	110[23]
Gut Fluid		146[c]		
Gut Tissue	20.6			
Muscle Fluid		146[24]		
Muscle Tissue	20.6			
Adipose Fluid		73[24]		
Adipose Tissue	20.6			
Rest of Body Fluid		73[c]		
Rest of Body Tissue	20.6			

[a] Total protein content of liver, kidney and gut were estimated based on a study that investigated the distribution of heart FABP in different organs; in that study, heart FABP concentrations were normalized to both protein content and organ weight; based on that information the protein content of each tissue could be determined. For other tissues the same protein concentration as that in gut was assumed.

[b] Calculated assuming molecular weight of albumin is 65 kg/mol[25].

[c] Kidney and gut were assumed to have similar albumin levels as liver and the "rest of body" was the same as muscle.

[d] Calculated assuming molecular weight of L-FABP is 14 kg/mol[23].

[e] α2u-globulin is a male-specific protein and its molecular weight is 15.5 kg/mol[23].

S2-2. Protein binding.

Table S3. Association constants (K_a) and binding sites (n) for PFOA binding to proteins and their sources.

	K_a (M^{-1})	n	Source
Albumin	3.1×10^3	7.8	Han et al. (2003)[26]
L-FABP[a]	1.2×10^5 4.0×10^4 1.9×10^4	3	Woodcroft et al. (2010)[27]
α2u-globulin	5.0×10^2	1	Han et al. (2004)[28]

[a] Based on Woodcroft et al.[27], three binding sites exist for L-FABP interacting with PFOA, with association constants of 1.2×10^5, 4.0×10^4 and 1.9×10^4 M^{-1}.

We used the equilibrium association constant (K_a) to derive individual rate constants for protein binding and dissociation (b_{on} and b_{off}) according to the same procedure described in the original fish model[6]. The equations used are listed below:

$$K_a = \frac{k_{on}^p}{k_{off}^p} \quad \text{(S1)}$$

$$\frac{dC_{unocc}^p}{dt} = k_{off}^p C_{bound} - k_{on}^p C_{unocc}^p C_{free} \quad \text{(S2)}$$

$$b_{on} = k_{on}^p C_{unocc}^p \quad \text{(S3)}$$

$$b_{off} = k_{off}^p \quad \text{(S4)}$$

Where:

k_{on}^p – association rate constant, $M^{-1}s^{-1}$.

k_{off}^p – dissociation rate constant, s^{-1}.

C_{unocc}^p – concentration of unoccupied binding sites of protein p.

C_{bound} – concentration of PFOA bound to protein.

C_{free} – concentration of free PFOA.

b_{on} – PFOA binding rate constant, s^{-1}.

b_{off} – rate constant for dissociation from protein, s^{-1}.

The initial concentration of unoccupied binding sites is the total concentration of protein in each compartment times the number of binding sites per protein molecule. It has been demonstrated that steady-state solutions depend only on K_a but not on the individual association and dissociation rate constants (k_{on} and k_{off}), which means that we can set a fixed value (e.g. 0.01 s^{-1}) for k_{off} and use it to calculate k_{on} based on the above equations[6]. The parameter k_{off} was included in the model sensitivity analysis, assuming it is uniformly distributed from 0.001 s^{-1} to 0.1 s^{-1} in order to understand the influence of this parameter on the dynamic solutions in this study.

S2-3. Membrane transporters.

Table S4. Protein-facilitated PFOA uptake velocity for five transporters and their sources.

Transporters	*In vitro* net flux (nmol/mg protein/min)	Sources
Oat1	0.34	Weaver et al. (2010)[29]
Oat3	0.48	
Oatp1a1	0.35	
Ntcp	0.1	Zhao et al. (2015)[30]
Ostα/β	0.41	

The method used to extrapolate measured *in vitro* uptake rates to corresponding absorption and efflux rate constants in our model is explained in Section S3-3.

S3. Derivation of Rate Constants.

All methods and equations used in this section to derive rate constants were based on the original fish model[6] except for the active transport rate constant. We modified the original method for deriving the active transport parameters by taking into consideration the fact that the ratio of active uptake to passive diffusion rate is consistent under both *in-vitro* and *in-vivo* situations, as described in Section S3-3

below.

S3-1. Passive diffusion rate constants.

Before calculating the passive diffusion rate, the effective permeability for each tissue must be estimated. Based on the original fish model, a single cell with average surface area (A) of 4000 μm^2 was assumed to calculate permeability[6].

Table S5. Effective permeability (P_{eff}) for each tissue and steady-state cell-water concentration ratios (CR_{SS}^{C-W}).

Tissue	Blood	Liver	Kidney	Gut	Muscle	Adipose	Rest of Body
P_{eff} (m/s)	4.98e-08	5.15e-08	4.38e-08	2.65e-08	2.65e-08	2.65e-08	2.65e-08
CR_{SS}^{C-W}							
Hepatocyte to bile				7.28			
Kidney to filtrate				6.19			
Enterocyte to gut lumen				3.75			

According to Fick's Law, permeability is expressed as:

$$P_{eff} = \frac{J}{A\Delta C} \quad \text{(S5)}$$

J is the initial passive diffusion flux extracted from Weaver et al.[29] and it has an average value of 0.13 nmol/mg protein/min, which is converted to mol/s by scaling to tissue-specific protein content of each cell. ΔC is the concentration of PFOA in the exposure medium, which in Weaver et al. study was 10 μmol/L.

Once P_{eff} was determined, we calculated the passive diffusion rate as described below.

For diffusion between blood (B) and the interstitial fluid compartment in each tissue (*i*F), the overall mass transfer coefficients are:

$$k^{iF-B} = k^{B-iF} = \left(\frac{1}{Q_B^i} + \frac{1}{P_{eff}^B A^{B-iF}}\right)^{-1} \quad \text{(S6)}$$

Q_B^i is the blood flow to each tissue, and A^{B-iF} is the exchange area between blood and fluid compartment (Table S1). Then the passive diffusion rate constants can be

determined as:

$$b^{iF-B} = \frac{k^{iF-B}}{V^{iF}} \quad \text{(S7)}$$

$$b^{B-iF} = \frac{k^{B-iF}}{V^{B}} \quad \text{(S8)}$$

V^{B} and V^{iF} are the volume of blood and fluid compartment, respectively (Table S1).

For transport between the fluid (iF) and tissue (iT) subcompartment in each tissue, only permeability accounts for the overall mass transfer coefficients for passive diffusion:

$$k^{iF-iT} = k^{iT-iF} = P^{i}_{eff} A^{iF-iT} \quad \text{(S9)}$$

The passive diffusion rate constants are:

$$b^{iF-iT} = \frac{k^{iF-iT}}{V^{iF}} \quad \text{(S10)}$$

$$b^{iT-iF} = \frac{k^{iT-iF}}{V^{iT}} \quad \text{(S11)}$$

For tissues containing other subcompartments (iO), namely, filtrate, bile, or gut lumen, the overall mass transfer coefficients are:

$$k^{iO-iT} = P^{i}_{eff} A^{iT-iO} \quad \text{(S12)}$$

$$k^{iT-iO} = \frac{k^{iO-iT}}{CR_{ss}^{C-W}} \quad \text{(S13)}$$

CR_{ss}^{C-W} is the steady-state cell-water concentration ratio, which was estimated using the data of Weaver et al[29]. The steady-state concentration in the cells was determined by extrapolating their concentration to very long times (> 10^6 min) and the concentration in the medium was assumed to be constant (10 μmol/L)[6].

The passive diffusion rate constants for these tissues are:

$$b^{iT-iO} = \frac{k^{iT-iO}}{V^{iT}} \quad \text{(S14)}$$

$$b^{iO-iT} = \frac{k^{iO-iT}}{V^{iO}} \quad \text{(S15)}$$

S3-2. Protein binding and dissociation rate constants.

See Section S2-2.

S3-3. Active transport rate constants.

Table S6. *In vitro-in vivo* extrapolation of transporter-mediated uptake and efflux rate constants (b) of PFOA.

Transporters	***In vivo* transport rate constants b (s^{-1})**[a]	
	Kidney	**Liver**
Oat1	0.03	
Oat3	0.04	
Oatp1a1	0.15	0.07
Ntcp[b]		0.02
Ostα/β[b]	0.01	

[a] All rate constant values shown here are calculated by assuming the body weight of rat is 250g.

[b] Only kinetics of transporting PFOS was reported[30]. We assume the same kinetics for PFOA.

To keep consistent ratios of active transport and passive diffusion before and after derivation from *in-vitro* studies, we used the similar method as deriving passive diffusion rate constants to estimate the active transport rate constants. Instead of using the flux measured in empty vector-transfected cells, the net flux (Table S4), which is the difference between the flux of transporter-expressing cell and the empty vector-transfected cell, was applied to obtain the active transport coefficient based on Equation (S5). Active transport rate constants can be determined from the transport coefficient multiplied by the surface area for exchange and then divided by the corresponding compartment volume.

In kidney tissue, Oat1 and Oat3, located at the basolateral membrane of proximal tubules are responsible for the clearance of PFOA from kidney to urine (b_{clear})[31]:

$$b_{clear} = b^{K}_{oat1} + b^{K}_{oat3} \quad \text{(S16)}$$

While Oatp1al, located on the apical membrane drives reabsorption of PFOA from urine back to systemic circulation (b_{reab})[31]:

$$b_{reab} = b^{K}_{oatp1a1} \quad \text{(S17)}$$

Another transporter, Ostα/β, was also considered for the male rat, which may account for some of the observed gender differences[32]. Ostα/β is located on the basolateral membrane and could excrete PFOA out of proximal tubules[31]. The efflux rate constant (b_{efflux}) is:

$$b_{efflux} = b^{K}_{ost\alpha/\beta} \quad \text{(S18)}$$

In liver tissue, two basolateral membrane transporters, Ntcp and Oatp1a1 could facilitate the PFOA uptake process[30], and the absorption rate constant (b_{abs}) is:

$$b_{abs} = b^{L}_{oatp1a1} + b^{L}_{Ntcp} \quad \text{(S19)}$$

Unlike passive diffusion, all active transport processes are assumed to be unidirectional in our model.

S4 Sensitivity and Uncertainty Analysis.

Our model contains a total of 74 parameters for predicting the distribution of PFOA in rats. Scaling functions were used to estimate the physiological parameters such as tissue volume and blood flow rate. The volume fraction of "rest of body" and the blood flow to "rest of body" were calculated by subtracting the fraction of other tissues from 1. Given this reparameterization, 72 independent parameters were included in the model. To conduct uncertainty and sensitivity analysis, all parameters were sampled from uniform, normal or log-normal distributions. Body weight and dose were assumed to be normally distributed, and their means were estimated as the

average values from corresponding experimental studies with a coefficient of variation (CV) of 0.15, estimated based on Kemper's study[33], where the data of body weight of individual rat and actual dose used in each experiment were available. Another parameter related to protein binding, the dissociation rate constant, k_{off}, was sampled from a uniform distribution ranging from 0.001 s^{-1} to 0.1 s^{-1}, since no studies currently exist to measure this parameter. All other parameters were assumed to be log-normally distributed, with the values collected from the literature used as the geometric means (e^{μ}, where μ is the mean of the corresponding normal distribution) for each parameter; and the geometric standard deviation (e^{σ}, where σ is the standard deviation of the corresponding normal distribution) were assumed based on confidence factors (Cf). The Cf is an intuitive measure of variance in log-normal distributions[34]. For example, a Cf of 2 indicates that 95% of the values lie between 1/2 and 2 times the median. According to the assumed Cf of each input parameter (Table S7), σ can be determined as[34]:

$$\sigma = \frac{1}{2}\ln Cf \qquad \text{(S20)}$$

Table S7 summarizes the geometric mean and assumed Cf for each parameter as well as the argument to estimate those parameters. For Cf, a value of 3 indicate fairly high uncertainty as it assumes a range of about one order of magnitude. We therefore chose a Cf of 3 when few or no data were available for estimation of uncertainty or variability.

The sensitivity of the model to each parameter was estimated based on correlation analysis, as shown in Figures S1-S3.

Table S7. Assumed confidence factors (Cf) for input parameters in the model.

Parameter	Value	Assumed Cf	Arguments to estimate each Cf		Notes
			Range		
			Lower	Upper	
Rat physiology					
Blood volume (VB)	5.4 %BW	1.7	-	-	The range of kidney, liver, gut, muscle, and adipose volume were obtained from Brown et al.[2]. Their corresponding Cf values were calculated based on the 2.5th and 97.5th percentile, which were assumed to be the lower and upper bound, respectively. For other tissue volume parameters, we assumed the Cfs were the same as the largest Cf value of adipose volume. The range of adipose is based on mouse data.
Plasma volume (Vplasma)	3.12 %BW	1.7	-	-	
Kidney volume (VK)	0.73 %BW	1.4	0.49	0.91	
Liver volume (VL)	3.66 %BW	1.6	2.14	5.16	
Gut volume (VG)	2.69 %BW	1.4	2	4	
Muscle volume (VM)	40.43 %BW	1.1	35.36	45.5	
Adipose volume (VA)	7 %BW	1.7	5	14	
Filtrate volume (VFil)	0.25 mL	1.7	-	-	
Bile duct volume (Vbile)	0.4 % liver tissue	1.7	-	-	
Gut lumen volume (VGL)	4.5 %BW	1.7	-	-	
Kidney blood volume (VKB)	0.16 mL/g tissue	1.6	0.11	0.27	The range of kidney, liver and muscle blood volume were obtained from Brown et al.[2]. For gut, muscle, adipose, and "rest of body" blood volume and liver and muscle interstitial volume, the same assumptions as above were made to estimate their Cf values. While for kidney, gut, adipose, and the "rest of body" interstitial volume, since their values are relatively large, we assumed their Cfs to be either 1.5 or 1.6 given that these fractional values must be less than 1 mL/g tissue.
Liver blood volume (VLB)	0.21 mL/g tissue	1.5	0.12	0.27	
Gut blood volume (VGB)	0.034 mL/g tissue	3	-	-	
Muscle blood volume (VMB)	0.04 mL/g tissue	3	0.01	0.09	
Adipose blood volume (VAB)	0.02 mL/g tissue	3	-	-	
Rest of body blood volume (VRB)	0.036 mL/g tissue	3	-	-	
Kidney interstitial fluid volume (VKF)	0.13 mL/g tissue	1.6	-	-	
Liver interstitial fluid volume (VLF)	0.049 mL/g tissue	3	-	-	
Gut interstitial fluid volume (VGF)	0.28 mL/g tissue	1.5	-	-	
Muscle interstitial fluid volume (VMF)	0.054 mL/g tissue	3	-	-	
Adipose interstitial fluid volume (VAF)	0.174 mL/g tissue	1.6	-	-	
Rest of body interstitial fluid volume (VRF)	0.18 mL/g tissue	1.6	-	-	

Parameters	Values	Assumed Cf	Arguments to estimate each Cf		Notes
			Range		
			Lower	Upper	
Blood flow to kidney (QBK)	14.1 % Cardiac Output	1.4	9.5	19	The range of blood flow to kidney, liver and gut came from Brown et al.[2]. For QGFR, Qurine, Qbile, and Qfeces, we assumed their Cfs to be the same as the largest Cf value of QBL. While for QBM and QBA, as their values are constrained to be less than 1, we assumed their Cfs were 1.3.
Blood flow to liver (QBL)	2.4 % Cardiac Output	2.7	0.8	5.8	
Blood flow to gut (QBG)	15.1 % Cardiac Output	1.3	11.1	17.8	
Blood flow to muscle (QBM)	27.8 % Cardiac Output	1.3	-	-	
Blood flow to adipose (QBA)	7 % Cardiac Output	1.3	-	-	
Glomerular filtration rate (QGFR)	10.74 mL/min/kg BW	2.7	-	-	
Urine flow rate (Qurine)	200 mL/d/kg BW	2.7	-	-	
Bile flow rate (Qbile)	90 mL/d/kg BW	2.7	-	-	
Feces flow rate (Qfeces)	5.63 mL water/day	2.7	-	-	
Protein binding					
Albumin concentration in blood (C_{AlbB})	486 µmol/L	3	-	-	No data on the range of protein content in tissues were available. We assume Cf values of 3 for all protein concentration parameters.
Albumin concentration in kidney fluid (C_{AlbKF})	243 µmol/L	3	-	-	
Albumin concentration in liver fluid (C_{AlbLF})	243 µmol/L	3	-	-	
Albumin concentration in gut fluid (C_{AlbGF})	146 µmol/L	3	-	-	
Albumin concentration in muscle fluid (C_{AlbMF})	146 µmol/L	3	-	-	
Albumin concentration in adipose fluid (C_{AlbAF})	73 µmol/L	3	-	-	
Albumin concentration in rest of body fluid (C_{AlbRF})	73 µmol/L	3	-	-	
L-FABP concentration in kidney tissue ($C_{LFABPKT}$)	2.65 µmol/L	3	-	-	
L-FABP concentration in liver tissue ($C_{LFABPLT}$)	133 µmol/L	3	-	-	
α2u-globulin concentration in kidney tissue ($C_{α2uKT}$)	110 µmol/L	3	-	-	
Association constant of albumin (K_a)	3.1×10^3 M^{-1}	3.5	2.6×10^3	3.12×10^4	The range for K_a was estimated based on data from human serum albumin[35].
Association constant of L-FABP binding site 1 (K_{LFABP1})	1.2×10^5 M^{-1}	3.5	-	-	
Association constant of L-FABP binding site 2 (K_{LFABP2})	4.0×10^4 M^{-1}	3.5	-	-	
Association constant of L-FABP binding site 3 (K_{LFABP3})	1.9×10^4 M^{-1}	3.5	-	-	
Association constant of α2u-globulin ($K_{α2u}$)	5.0×10^2 M^{-1}	3.5	-	-	

Parameters	Values	Assumed Cf	Arguments to estimate each Cf		Notes
			Range		
			Lower	Upper	
Passive diffusion and Active transport					
Capillary surface area of kidney (AK)	350 cm^2/g tissue	3	-	-	No data were available on the range of surface area parameters. We assume Cf values of 3 for all of them.
Glomerular capillary surface area in kidney (AKG)	6890 mm^2/g tissue	3	-	-	
Enlargement factor of apical membrane of proximal tubule (n)	5	3	-	-	
Capillary surface area of liver (AL)	250 cm^2/g tissue	3	-	-	
Capillary surface area of gut (AG)	100 cm2/g tissue	3	-	-	
Capillary surface area of gut lumen (AGL)	4.14 m^2/kg BW	3	-	-	
Capillary surface area of muscle(AM)	70 cm^2/g tissue	3	-	-	
Capillary surface area of adipose (AA)	70 cm^2/g tissue	3	-	-	
Capillary surface area of rest of body (AR)	100 cm^2/g tissue	3	-	-	
Effective permeability for blood (P_{effB})	4.98×10^{-8} m/s	5	-	-	The Cf values for permeability and active transport parameters were assumed to be the same as the value used in the Yang. et al.[36] study.
Effective permeability for kidney (P_{effK})	4.38×10^{-8} m/s	5	-	-	
Effective permeability for liver (P_{effL})	5.15×10^{-8} m/s	5	-	-	
Effective permeability for gut (P_{effG})	2.65×10^{-8} m/s	5	-	-	
Effective permeability for muscle (P_{effM})	2.65×10^{-8} m/s	5	-	-	
Effective permeability for adipose (P_{effA})	2.65×10^{-8} m/s	5	-	-	
Effective permeability for rest of body (P_{effR})	2.65×10^{-8} m/s	5	-	-	
Steady-state cell-water concentration ratio for kidney ($CR_{ss}K$)	6.19	5	-	-	
Steady-state cell-water concentration ratio for liver ($CR_{ss}L$)	7.28	5	-	-	
Steady-state cell-water concentration ratio for gut ($CR_{ss}G$)	3.75	5	-	-	
Renal clearance rate constant (b_{clear})	0.07 s^{-1}	5	-	-	
Renal reabsorption rate constant (b_{reab})	0.15 s^{-1}	5	-	-	
Renal efflux rate constant (b_{efflux})	0.01 s^{-1}	5	-	-	

Absorption rate constant of hepatocyte (b_{abs})	0.09 s^{-1}	5	-	-

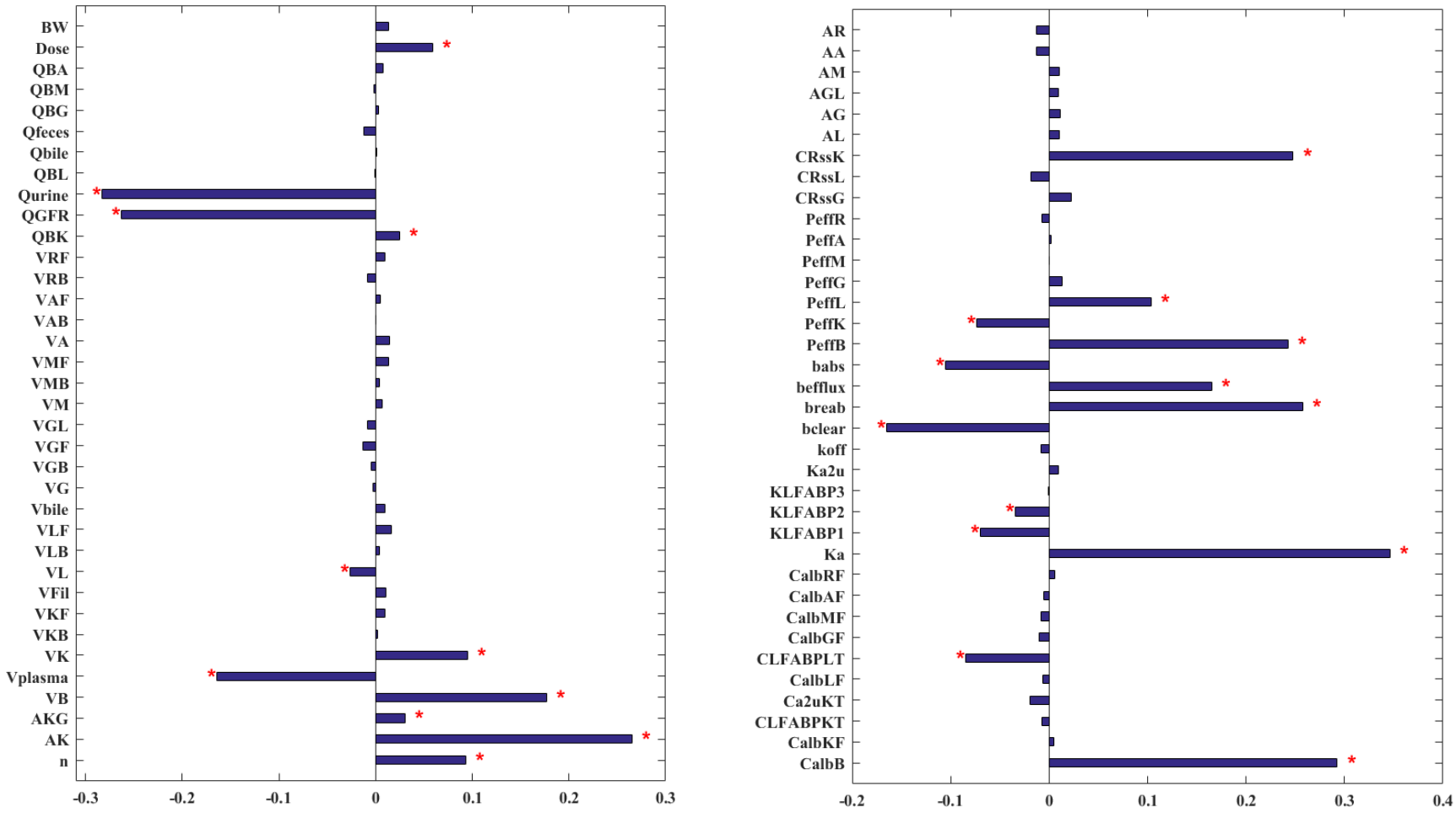

Figure S1. Correlation analysis between each sampled model parameter and PFOA concentration in blood after 12 days. '*' indicates $P < 0.05$. The correlation coefficient is the average of three simulation results at different dose and administration routes (1 mg/kg oral dose, 1 mg/kg IV dose and 0.1 mg/kg oral dose), given that the sensitivities were similar for the three scenarios.

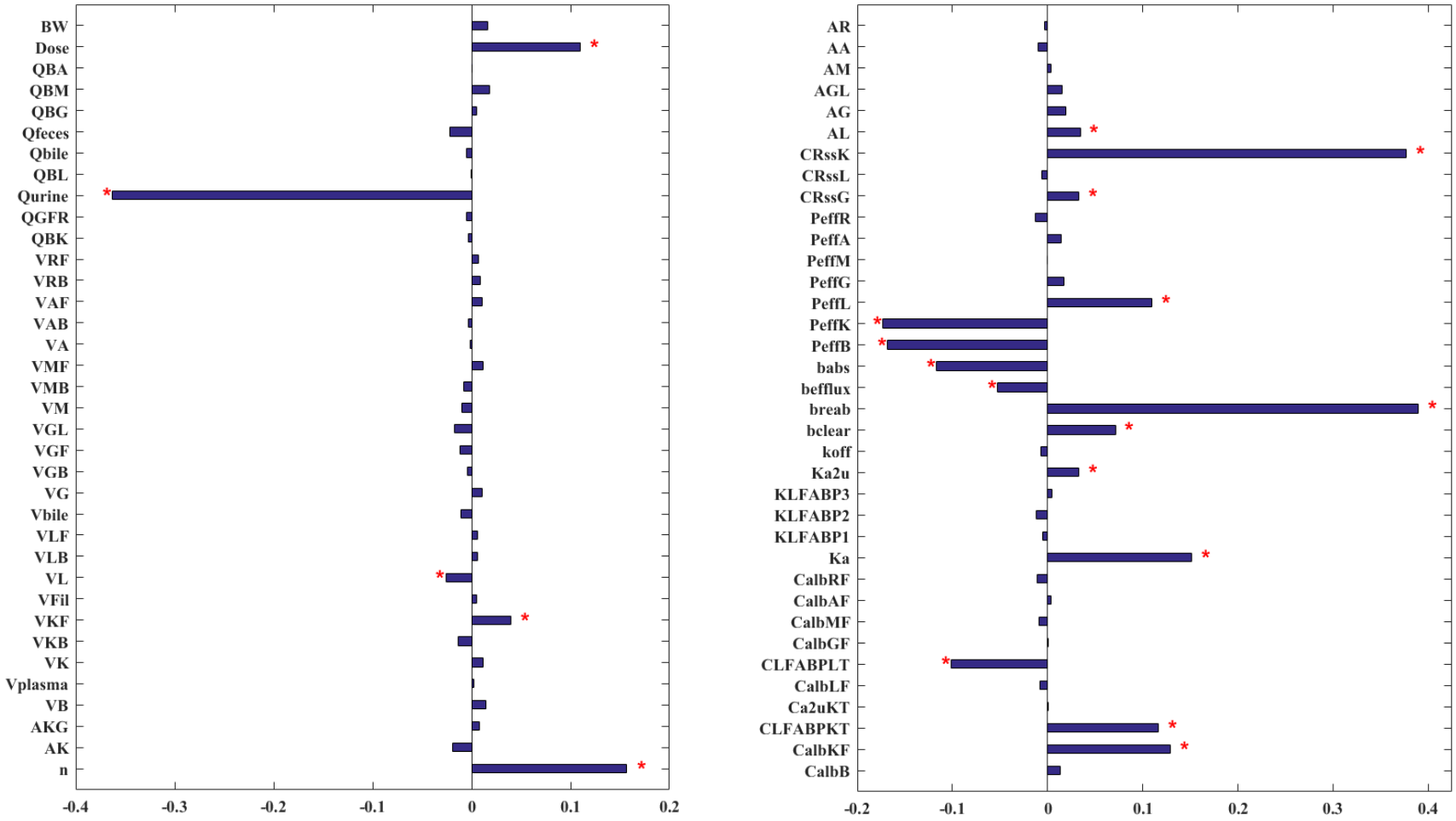

Figure S2. Correlation analysis between each sampled model parameter and PFOA concentration in kidney after 12 days. '*' indicates $P < 0.05$. Correlation coefficient is the average of three simulation results at different dose and administration routes (1 mg/kg oral dose, 1 mg/kg IV dose and 0.1 mg/kg oral dose), given that the sensitivities were similar for the three scenarios.

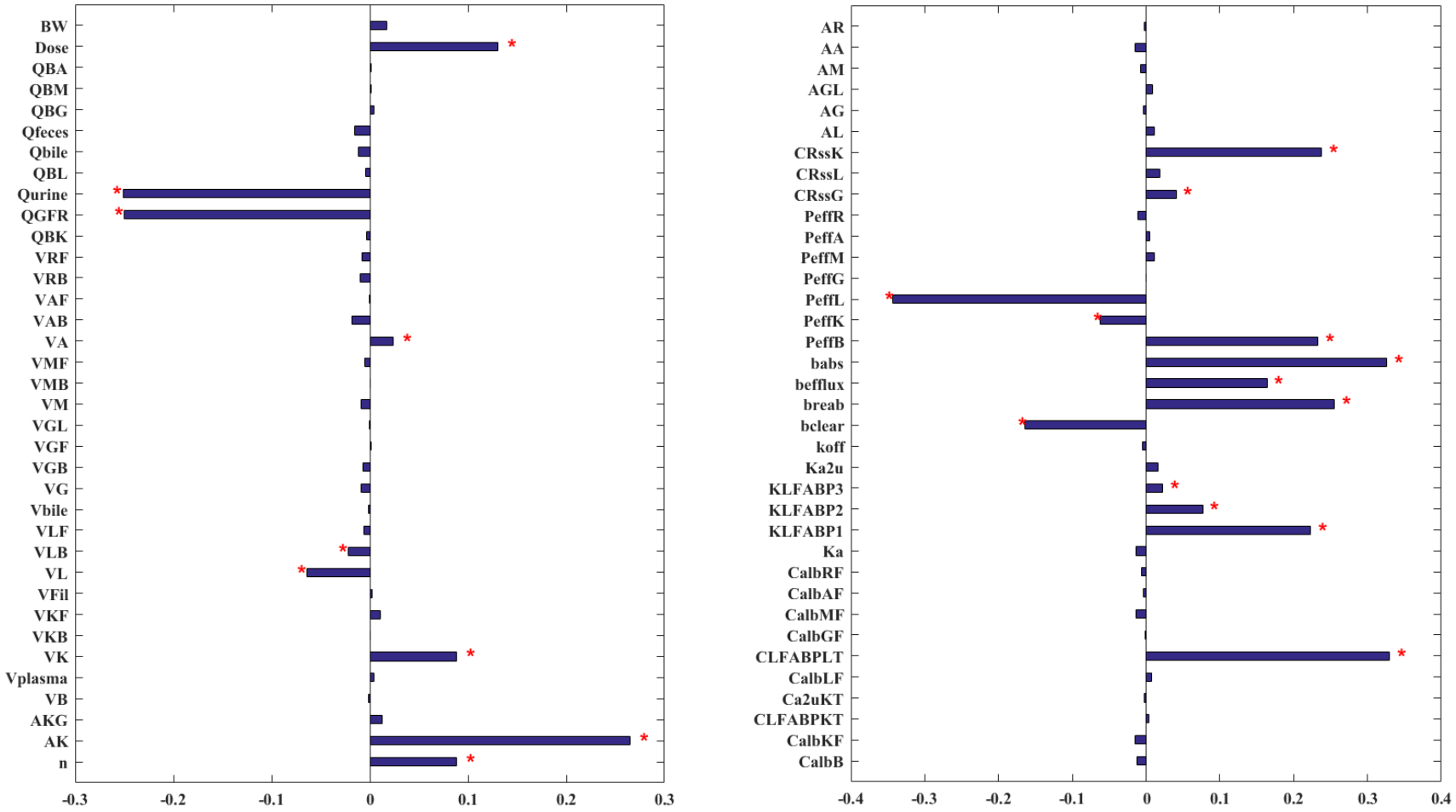

Figure S3. Correlation analysis between each sampled model parameter and PFOA concentration in liver after 12 days. '*' indicates $P < 0.05$. Correlation coefficient is the average of three simulation results at different dose and administration routes (1 mg/kg oral dose, 1 mg/kg IV dose and 0.1 mg/kg oral dose), given that the sensitivities were similar for the three scenarios.

S5 PFOA Concentration Profile in Compartments.

The predicted PFOA concentration profile in tissue compartments for different dose scenarios are shown in Figures S4-S6. We only had experimental data at single time points, but here we show model prediction as a function of time and can show that experimental data fall within the 95% confidence interval.

Standard toxicokinetic parameters were also calculated based on model predictions (Table S8).

Table S8. Toxicokinetic parameters comparison between prediction and experimental data

Toxicokinetic parameters	01ppm oral[a]		1ppm oral[a]		1ppm IV[a]	
	predicted value	experimental data	predicted value	experimental data	predicted value	experimental data
Cmax (ng/g)	311.20	598±127	2810.00	8431±1161	-	-
Tmax (h)	5.80	10.25±6.45	5.80	9.00±3.83	-	-
half-life (day)	6.80	8.41±1.56	6.93	5.76±1.33	6.93	7.73±0.82
Clearance (mL/kg/day)	62.67	23.10±5.76	69.64	20.9±3.79	69.45	21.51±1.97

[a] the experimental data are extracted from the Kemper study[33]

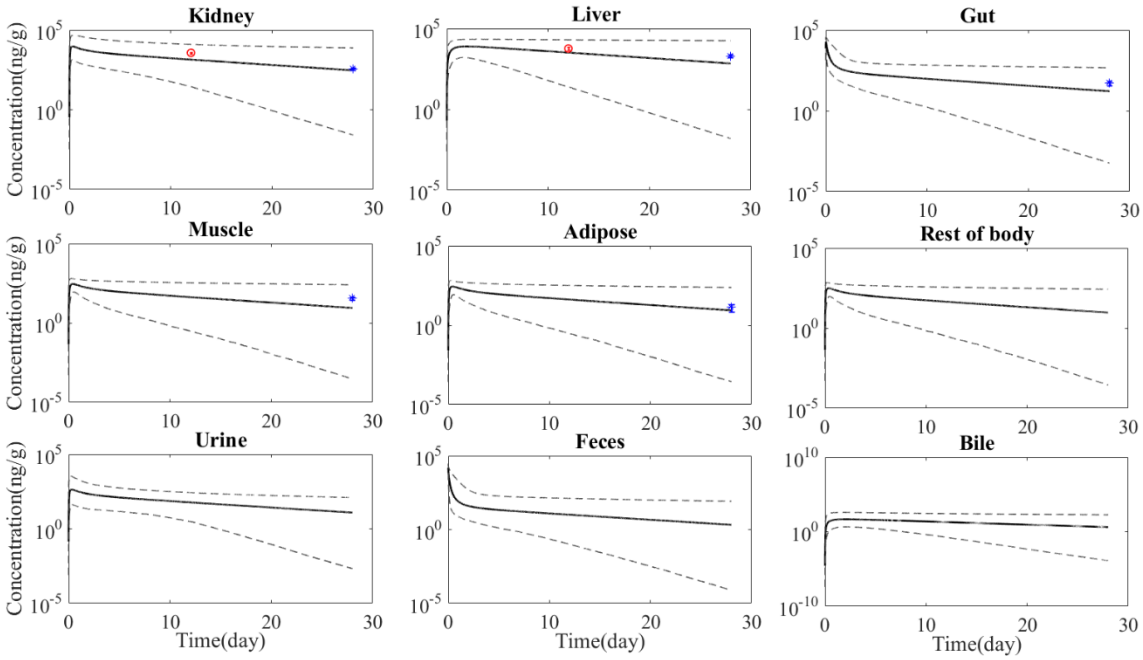

Figure S4. Concentration profile as a function of time for PFOA in different compartments after a single oral dose of 1 mg/kg. The upper and lower dotted lines represent the 97.5th percentile and 2.5th percentile of predicted results, respectively; the solid line corresponds to geometric mean values. 'o' is the experimental data from the Kim et al[37] study, and '*' indicates the data from the Kemper's[33] study.

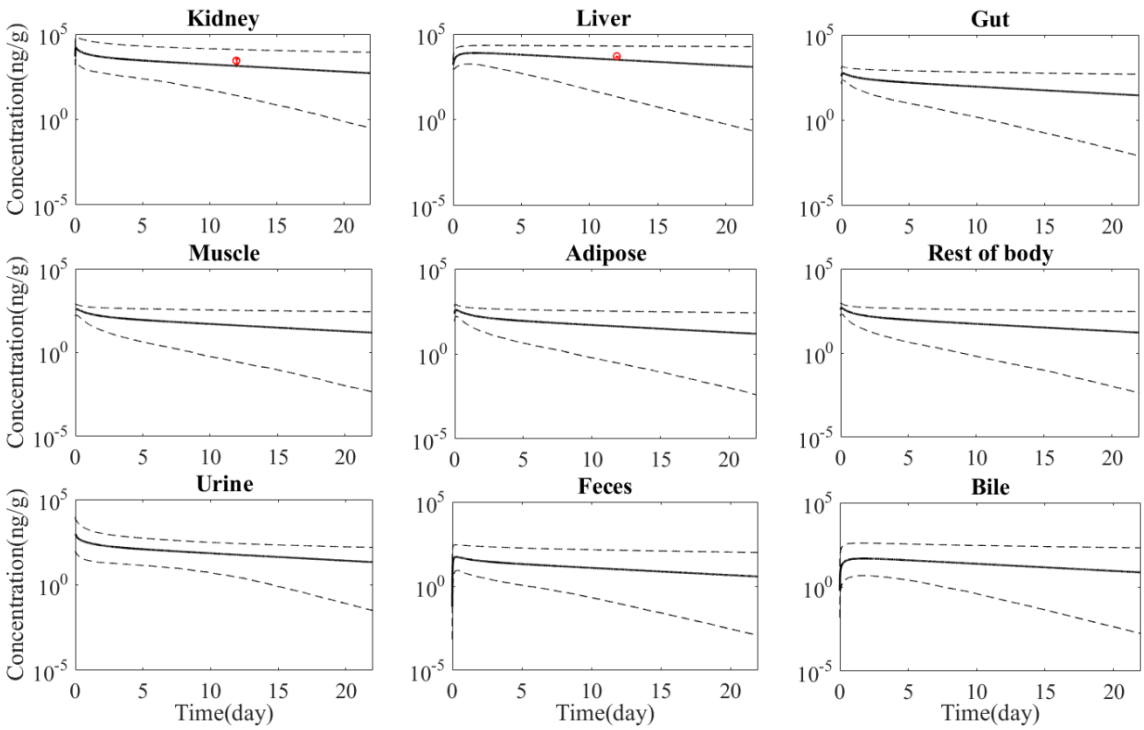

Figure S5. Concentration profile as a function of time for PFOA in different compartments after a single IV dose of 1 mg/kg. The upper and lower dotted lines represent the 97.5th percentile and 2.5th percentile of predicted results, respectively; the solid line corresponds to geometric mean values. 'o' is the experimental data from the Kim et al[37] study.

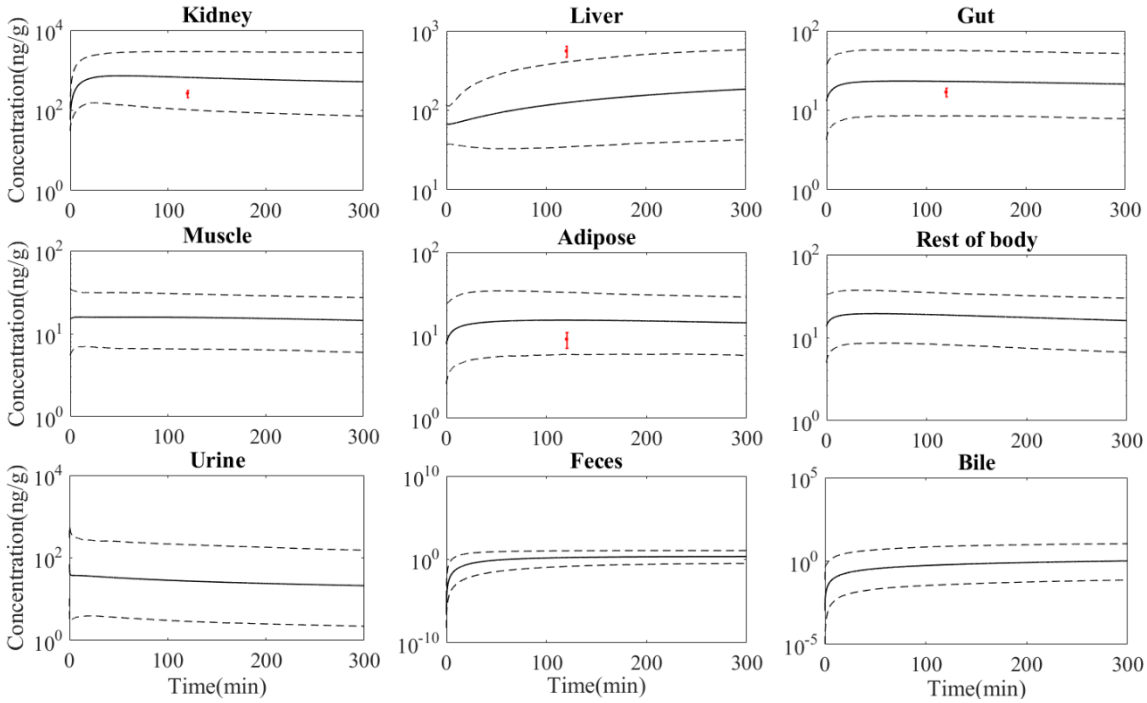

Figure S6. Concentration profile as a function of time for PFOA in different compartments after a single IV dose of 0.041 mg/kg. The upper and lower dotted lines represent the 97.5th percentile and 2.5th percentile of predicted results, respectively; the solid line corresponds to geometric mean values. Red dot indicates the experimental data from the Kudo et al.[38] study.

S6 PBPK Model Code.

The PBPK model developed in this study was programmed in MATLAB (MATLAB R2016a); the code for the Kemper IV dose simulation follows as an illustrative example.

References

(1) Davies, B.; Morris, T. Physiological parameters in laboratory animals and humans. *Pharm. Res.* **1993,** *10* (7), 1093-1095.

(2) Brown, R. P.; Delp, M. D.; Lindstedt, S. L.; Rhomberg, L. R.; Beliles, R. P. Physiological parameter values for physiologically based pharmacokinetic models. *Toxicol. Ind. Health* **1997,** *13* (4), 407-484.

(3) Blouin, A.; Bolender, R. P.; Weibel, E. R. Distribution of organelles and membranes between hepatocytes and nonhepatocytes in the rat liver parenchyma. A stereological study. *J. Cell Biol.* **1977,** *72* (2), 441-455.

(4) Larson, M.; Sjöquist, M.; Wolgast, M. Renal interstitial volume of the rat kidney. *Acta Physiol. Scand.* **1984,** *120* (2), 297-304.

(5) Barratt, T. M.; Walser, M. Extracellular fluid in individual tissues and in whole animals: the distribution of radiosulfate and radiobromide. *J. Clin. Invest.* **1969,** *48* (1), 56.

(6) Ng, C. A.; Hungerbühler, K. Bioconcentration of perfluorinated alkyl acids: how important is specific binding? *Environ. Sci. Technol.* **2013,** *47* (13), 7214-7223.

(7) Everett, N. B.; Simmons, B.; Lasher, E. P. Distribution of blood (Fe59) and plasma (I131) volumes of rats determined by liquid nitrogen freezing. *Circul. Res.* **1956,** *4*, 419-424.

(8) Crone, C. The permeability of capillaries in various organs as determined by use of the 'indicator diffusion'method. *Acta Physiol. Scand.* **1963,** *58* (4), 292-305.

(9) McConnell, E. L.; Basit, A. W.; Murdan, S. Measurements of rat and mouse gastrointestinal pH, fluid and lymphoid tissue, and implications for in‐vivo experiments. *J. Pharm. Pharmacol.* **2008,** *60* (1), 63-70.

(10) Munger, K.; Baylis, C. Sex differences in renal hemodynamics in rats. *Am. J. Physiol. Renal Physiol.* **1988,** *254* (2), F223-F231.

(11) Biewald, N.; Billmeier, J. Blood volume and extracellular space (ECS) of the whole body and some organs of the rat. *Experientia* **1978,** *34* (3), 412-413.

(12) Kirkman, H.; Stowell, R. Renal filtration surface in the albino rat. *Anat. Rec.* **1942,** *82* (3), 373-391.

(13) DeSesso, J.; Jacobson, C. Anatomical and physiological parameters affecting gastrointestinal absorption in humans and rats. *Food Chem. Toxicol.* **2001,** *39* (3), 209-228.

(14) Arthur, S.; Green, R. Fluid reabsorption by the proximal convoluted tubule of the kidney in lactating rats. *J. Physiol.* **1986,** *371*, 267.

(15) Bonvalet, J.; de Rouffignac, C. Distribution of ferrocyanide along the proximal tubular lumen of the rat kidney: its implications upon hydrodynamics. *J. Physiol.* **1981,** *318*, 85.

(16) Frazier, K. S.; Seely, J. C.; Hard, G. C.; Betton, G.; Burnett, R.; Nakatsuji, S.; Nishikawa, A.; Durchfeld-Meyer, B.; Bube, A. Proliferative and nonproliferative lesions of the rat and mouse urinary system. *Toxicol. Pathol.* **2012,** *40* (4 suppl), 14S-86S.

(17) Kanauchi, O.; Agata, K.; Fushiki, T. Mechanism for the increased defecation and jejunum mucosal protein content in rats by feeding germinated barley foodstuff. *Biosci., Biotechnol., Biochem.* **1997,** *61* (3), 443-448.

(18) Cavigelli, S.; Monfort, S.; Whitney, T.; Mechref, Y.; Novotny, M.; McClintock, M. Frequent serial fecal corticoid measures from rats reflect circadian and ovarian corticosterone rhythms. *J. Endocrinol.* **2005,** *184* (1), 153-163.

(19) Crisman, T. S.; Claffey, K. P.; Saouaf, R.; Hanspal, J.; Brecher, P. Measurement of rat heart fatty acid binding protein by ELISA. Tissue distribution, developmental changes and subcellular distribution. *J. Mol. Cell. Cardiol.* **1987,** *19* (5), 423-431.

(20) Levitt, D. G. The pharmacokinetics of the interstitial space in humans. *BMC Clin. Pharmacol.* **2003,** *3* (1), 3.

(21) Ockner, R. K.; Manning, J.; Kane, J. Fatty acid binding protein. Isolation from rat liver, characterization, and immunochemical quantification. *J. Biol. Chem.* **1982,** *257* (13), 7872-7878.

(22) Maatman, R. G.; van de Westerlo, E. M.; Van Kuppevelt, T.; Veerkamp, J. H. Molecular identification of the liver-and the heart-type fatty acid-binding proteins in human and rat kidney. Use of the reverse transcriptase polymerase chain reaction. *Biochem. J.* **1992,** *288* (1), 285-290.

(23) Kimura, H.; Odani, S.; Nishi, S.; Sato, H.; Arakawa, M.; Ono, T. Primary structure and cellular distribution of two fatty acid-binding proteins in adult rat kidneys. *J. Biol. Chem.* **1991,** *266* (9), 5963-5972.

(24) Ellmerer, M.; Schaupp, L.; Brunner, G. A.; Sendlhofer, G.; Wutte, A.; Wach, P.; Pieber, T. R. Measurement of interstitial albumin in human skeletal muscle and adipose tissue by open-flow microperfusion. *Am. J. Physiol. Endocrinol. Metab.* **2000,** *278* (2), E352-E356.

(25) Peters, T. The biosynthesis of rat serum albumin II. Intracellular phenomena in the secretion of newly formed albumin. *J. Biol. Chem.* **1962,** *237* (4), 1186-1189.

(26) Han, X.; Snow, T. A.; Kemper, R. A.; Jepson, G. W. Binding of perfluorooctanoic acid to rat and human plasma proteins. *Chem. Res. Toxicol.* **2003,** *16* (6), 775-781.

(27) Woodcroft, M. W.; Ellis, D. A.; Rafferty, S. P.; Burns, D. C.; March, R. E.; Stock, N. L.; Trumpour, K. S.; Yee, J.; Munro, K. Experimental characterization of the mechanism of perfluorocarboxylic acids' liver protein bioaccumulation: The key role of the neutral species. *Environ. Toxicol. Chem.* **2010,** *29* (8), 1669-1677.

(28) Han, X.; Hinderliter, P. M.; Snow, T. A.; Jepson, G. W. Binding of Perfluorooctanoic Acid to Rat Liver - form and Kidney - form α 2u - Globulins. *Drug Chem. Toxicol.* **2004,** *27* (4), 341-360.

(29) Weaver, Y. M.; Ehresman, D. J.; Butenhoff, J. L.; Hagenbuch, B. Roles of rat renal organic anion transporters in transporting perfluorinated carboxylates with different chain lengths. *Toxicol. Sci.* **2009**, kfp275.

(30) Zhao, W.; Zitzow, J. D.; Ehresman, D. J.; Chang, S.-C.; Butenhoff, J. L.; Forster, J.; Hagenbuch, B. Na+/taurocholate cotransporting polypeptide and apical sodium-dependent bile acid transporter are involved in the disposition of perfluoroalkyl sulfonates in humans and rats. *Toxicol. Sci.* **2015**, kfv102.

(31) Han, X.; Nabb, D. L.; Russell, M. H.; Kennedy, G. L.; Rickard, R. W. Renal elimination of perfluorocarboxylates (PFCAs). *Chem. Res. Toxicol.* **2011,** *25* (1), 35-46.

(32) Yang, C.-H.; Glover, K. P.; Han, X. Characterization of cellular uptake of perfluorooctanoate via organic anion-transporting polypeptide 1A2, organic anion transporter 4, and urate transporter 1 for their potential roles in mediating human renal reabsorption of perfluorocarboxylates. *Toxicol. Sci.* **2010,** *117* (2), 294-302.

(33) Kemper, R. A. Perfluorooctanoic acid: toxicokinetics in the rat. *Project ID: DuPont* **2003,** *7473*.

(34) MacLeod, M.; Fraser, A. J.; Mackay, D. Evaluating and expressing the propagation of uncertainty in chemical fate and bioaccumulation models. *Environ. Toxicol. Chem.* **2002,** *21* (4), 700-709.

(35) Hebert, P. C.; MacManus-Spencer, L. A. Development of a fluorescence model for the binding of medium-to long-chain perfluoroalkyl acids to human serum albumin through a mechanistic evaluation of spectroscopic evidence. *Anal. Chem.* **2010,** *82* (15), 6463-6471.

(36) Yang, Y.; Xu, X.; Georgopoulos, P. G. A Bayesian population PBPK model for multiroute chloroform exposure. *J. Expo. Sci. Environ. Epidemiol.* **2010,** *20* (4), 326-341.

(37) Kim, S.-J.; Heo, S.-H.; Lee, D.-S.; Hwang, I. G.; Lee, Y.-B.; Cho, H.-Y. Gender differences in pharmacokinetics and tissue distribution of 3 perfluoroalkyl and polyfluoroalkyl substances in rats. *Food Chem. Toxicol.* **2016,** *97*, 243-255.

(38) Kudo, N.; Sakai, A.; Mitsumoto, A.; Hibino, Y.; Tsuda, T.; Kawashima, Y. Tissue distribution and hepatic subcellular distribution of perfluorooctanoic acid at low dose are different from those at high dose in rats. *Biol. Pharm. Bull.* **2007,** *30* (8), 1535-1540.

```
%% Diffusion-Limited PBPK for PFOA in Male Rats
%% Code written by Weixiao Cheng, University of Pittsburgh
%% Last Modified: 26 July, 2017

% The purpose of this model is to predict the toxicokinetics and tissue
% distributioin of PFOA in male rats without the need to fit experimental
% data.

% This version implements Monte Carlo uncertainty analysis. Parameter
% values are therefore chosen from distributions (normal, lognormal,
% or uniform, see SI Section S4 for details) over 10,000 iterations.

% The code below is parameterized to replicate the conditions of the 1 mg/kg
% IV dose experiment from Kemper (33).
% For the code for other dose experiments, the paramters including body
% weight(BW), Dose, and sampling time (seconds) need to be modified to
% corresponding values based on different studies. Moreover, the initial
% condition is different between IV and oral dose treatment. Namely, for IV
% dose, the initial concentration of PFOA in the blood compartment is Dose
% times BW (i.e., in line 311 , y1 = Dose.*BW.*ones([1,Q])), with PFOA
% concentration in other compartments being zero; for oral dose, the initial
% concentration of PFOA in the gut lumen compartment is Dose time BW
% (i.e.,in line 340, y26 = Dose.*BW.*ones([1,Q])), with PFOA in other
% compartments being zero.
clc;
clear all;
close all;
Q = 10000; % number of iterations for Monte Carlo analysis
BW = normrnd(0.244,37e-3,1,Q);% body weight (kg)
Dose = normrnd(1e-6,0.15e-6,1,Q);% the unit is kg PFOA/kg BW


% Volume of tissue i as percentage of body weight (PVi, unitless) and
% volume (Vi, m^3), assuming the density of tissue is 1e3 kg/m^3.
PVB = lognrnd(log(54e-6),0.5*log(1.7),1,Q);
VB = PVB.*BW; % blood volume
PVplasma = lognrnd(log(31.2e-6),0.5*log(1.7),1,Q);
Vplasma = PVplasma.*BW; % plasma volume
PVK = lognrnd(log(0.73/100/1e3),0.5*log(1.4),1,Q);
VK = PVK.*BW; % kidney volume
PVKB = lognrnd(log(0.16),0.5*log(1.6),1,Q);
VKB = PVKB.*PVK.*BW; % kidney blood volume
PVKF = lognrnd(log(0.13),0.5*log(1.6),1,Q);
VKF = PVKF.*PVK.*BW; % kidney interstitial fluid volume
VKT = VK - VKF; % kidney tissue volume
VFil = lognrnd(log(0.25/1e6),0.5*log(1.7),1,Q);% renal filtrate volume
PVL = lognrnd(log(3.66/100/1e3),0.5*log(1.6),1,Q);
VL = PVL.*BW; % liver volume
PVLB = lognrnd(log(0.21),0.5*log(1.5),1,Q);
VLB = PVLB.*PVL.*BW; % liver blood volume
PVLF = lognrnd(log(0.049),0.5*log(3),1,Q);
VLF = PVLF.*PVL.*BW; % liver interstitial fluid volume
VLT = VL - VLF; % liver tissue volume
PVbile = lognrnd(log(0.004),0.5*log(1.7),1,Q);
```

```
Vbile = PVbile.*PVL.*BW; % bile volume
PVG = lognrnd(log(2.69/100/1e3),0.5*log(1.4),1,Q);
VG = PVG.*BW; % gut volume
PVGB = lognrnd(log(0.034),0.5*log(3),1,Q);
VGB = PVGB.*PVG.*BW; % gut blood volume
PVGF = lognrnd(log(0.28),0.5*log(1.5),1,Q);
VGF = PVGF.*PVG.*BW; % gut interstitial fluid volume
VGT = VG - VGF; % gut tissue volume
PVGL = lognrnd(log(4.5/100/1e3),0.5*log(1.7),1,Q);
VGL = PVGL.*BW; % gut lumen volume
PVM = lognrnd(log(40.43/100/1e3),0.5*log(1.1),1,Q);
VM = PVM.*BW; % muscle volume
PVMB = lognrnd(log(0.04),0.5*log(3),1,Q);
VMB = PVMB.*PVM.*BW; % muscle blood volume
PVMF = lognrnd(log(0.054),0.5*log(3),1,Q);
VMF = PVMF.*PVM.*BW; % muscle interstitial fluid volume
VMT = VM - VMF; % muscle tissue volume
PVA = lognrnd(log(7/100/1e3),0.5*log(1.7),1,Q);
VA = PVA.*BW; % adipose volume
PVAB = lognrnd(log(0.02),0.5*log(3),1,Q);
VAB = PVAB.*PVA.*BW; % adipose blood volume
PVAF = lognrnd(log(0.174),0.5*log(1.6),1,Q);
VAF = PVAF.*PVA.*BW; % adipose interstitial fluid volume
VAT = VA - VAF; % adipose tissue volume
PVR = 1/1e3 - PVB - PVK - PVL - PVG - PVM - PVA;
VR = PVR.*BW; % volume of the rest of body
PVRB = lognrnd(log(0.036),0.5*log(3),1,Q);
VRB = PVRB.*PVR.*BW; % volume of the blood of the rest of body
PVRF = lognrnd(log(0.18),0.5*log(1.6),1,Q);
VRF = PVRF.*PVR.*BW; % interstitial fluid volume of the rest of body
VRT = VR - VRF; % tissue volume of the rest of body


% Capillary surface area for each tissue (Ai) as percentage of body weight
% or weight of corresponding tissue (PAi, unitless) and surface area (m^2).
PAK = lognrnd(log(350e-4),0.5*log(3),1,Q);
AK = PAK.*VK.*10^6; % kidney surface area
PAKG = lognrnd(log(6890/1e6),0.5*log(3),1,Q);
AKG = PAKG.*VK.*10^6; % the surface area of glomerular capillary
PAL = lognrnd(log(250e-4),0.5*log(3),1,Q);
AL = PAL.*VL.*10^6; % liver surface area
PAG = lognrnd(log(100e-4),0.5*log(3),1,Q);
AG = PAG.*VG.*10^6; % gut surface area
PAGL = lognrnd(log(4.14),0.5*log(3),1,Q);
AGL = PAGL.*BW; % gut lumen surface area
PAM = lognrnd(log(70e-4),0.5*log(3),1,Q);
AM = PAM.*VM.*10^6; % muscle surface area
PAA = lognrnd(log(70e-4),0.5*log(3),1,Q);
AA = PAA.*VA.*10^6; % adipose surface area
PAR = lognrnd(log(100e-4),0.5*log(3),1,Q);
AR = PAR.*VR.*10^6; % surface area of rest of body


% Effective permeability (Peff, in m/s) for blood (B), liver(L), kidney(K),
```

```
% gut(G),adipose(A), muscle(M), rest of body(R).
PeffB = lognrnd(log(4.98e-8),0.5*log(5),1,Q);
PeffK = lognrnd(log(4.38e-8),0.5*log(5),1,Q);
PeffL = lognrnd(log(5.15e-8),0.5*log(5),1,Q);
PeffG = lognrnd(log(2.65e-8),0.5*log(5),1,Q);
PeffA = lognrnd(log(2.65e-8),0.5*log(5),1,Q);
PeffM = lognrnd(log(2.65e-8),0.5*log(5),1,Q);
PeffR = lognrnd(log(2.65e-8),0.5*log(5),1,Q);

% Steady-state cell-water concentration ratios(CRss) for gut, liver, and
% kidney.
CRssG = lognrnd(log(3.75),0.5*log(5),1,Q);
CRssL = lognrnd(log(7.28),0.5*log(5),1,Q);
CRssK = lognrnd(log(6.19),0.5*log(5),1,Q);


% Blood flow rates (QBi, in m^3/s) to different tissues (i=L, K, G, A, M, R)
% as a percentage of cardiac output (Qcardiac), which itself is a function
% of body weight (BW).
Qcardiac = 0.235/60*1e-3*BW.^0.75;
PQBK = lognrnd(log(14.1/100),0.5*log(1.4),1,Q);
QBK = PQBK.*Qcardiac;
PQBG = lognrnd(log(15.1/100),0.5*log(1.3),1,Q);
QBG = PQBG.*Qcardiac;
PQBL = lognrnd(log(2.4/100),0.5*log(2.7),1,Q);
QBL = (PQBL+PQBG).*Qcardiac;
PQBM = lognrnd(log(27.8/100),0.5*log(1.3),1,Q);
QBM = PQBM.*Qcardiac;
PQBA = lognrnd(log(7/100),0.5*log(1.3),1,Q);
QBA = PQBA.*Qcardiac;
PQBR = 1 - PQBK - PQBG - PQBL - PQBM - PQBA;
QBR = PQBR.*Qcardiac;
% Flow rate of fluids including feces, bile, urine and glomerular filtration
% rate (GFR), in m^3/s.
Qfeces = lognrnd(log(5.63*1e-6/(24*3600)),0.5*log(2.7),1,Q);
PQbile = lognrnd(log(90),0.5*log(2.7),1,Q);
Qbile = PQbile.*BW.*1e-6/(24*3600);
PQurine = lognrnd(log(200),0.5*log(2.7),1,Q);
Qurine = PQurine.*BW.*1e-6/(24*3600);
PQGFR = lognrnd(log(10.74),0.5*log(2.7),1,Q);
QGFR = PQGFR.*BW.*1e-6/60;


% Albumin concentration in blood and interstitial fluid compartments(mol/m^3).
CalbB = lognrnd(log(281e-3*7.8),0.5*log(3),1,Q);
CalbKF = lognrnd(log(243e-3*7.8),0.5*log(3),1,Q);
CalbLF = lognrnd(log(243e-3*7.8),0.5*log(3),1,Q);
CalbGF = lognrnd(log(146e-3*7.8),0.5*log(3),1,Q);
CalbMF = lognrnd(log(146e-3*7.8),0.5*log(3),1,Q);
CalbAF = lognrnd(log(73e-3*7.8),0.5*log(3),1,Q);
CalbRF = lognrnd(log(73e-3*7.8),0.5*log(3),1,Q);

% Alpha2mu-globulin concentration in kidney tissue (mol/m^3).
Ca2uKT = lognrnd(log(110e-3),0.5*log(3),1,Q);
```

```
163
164 % LFABP concentration in kidney and liver tissue (mol/m^3).
165 CL_fabpKT = lognrnd(log(2.65e-3*3),0.5*log(3),1,Q);
166 CL_fabpKT1 = CL_fabpKT./3;
167 CL_fabpKT2 = CL_fabpKT./3;
168 CL_fabpKT3 = CL_fabpKT./3;
169 CL_fabpLT = lognrnd(log(133e-3*3),0.5*log(3),1,Q);
170 CL_fabpLT1 = CL_fabpLT./3;
171 CL_fabpLT2 = CL_fabpLT./3;
172 CL_fabpLT3 = CL_fabpLT./3;
173
174
175 % Equilibrium association constant (m^3/mol) for albumin(Ka), LFABP(KL_fabp),
176 % and alpha2mu-globulin(Ka2u). See SI section S2-2 for details.
177 Ka = lognrnd(log(3.1),0.5*log(3.5),1,Q);
178 KL_fabp1 = lognrnd(log(120),0.5*log(3.5),1,Q);
179 KL_fabp2 = lognrnd(log(40.0),0.5*log(3.5),1,Q);
180 KL_fabp3 = lognrnd(log(19.0),0.5*log(3.5),1,Q);
181 Ka2u = lognrnd(log(0.5),0.5*log(3.5),1,Q);
182 % Individual rate constants for association and dissociation(s^-1 and m^3/mol*s).
183 % Note kon/koff=Keq.
184 koff = unifrnd(0.001,0.1,1,Q); % assume koff is 0.01/s
185 kon = koff.*Ka;
186 kL_fabpon1 = koff.*KL_fabp1;
187 kL_fabpon2 = koff.*KL_fabp2;
188 kL_fabpon3 = koff.*KL_fabp3;
189 kK_fabpon = koff.*Ka2u;
190
191
192 % Overall mass transfer coefficients between subcompartments and passive
193 % diffusion rate constants. See SI section S3-1 for details.
194 kBKF = ((1./QBK) + 1./(PeffB.*AK)).^(-1);
195 kBF =  PeffB.*AKG;
196 kKFKT = PeffK.*AK;
197 n = lognrnd(log(5),0.5*log(3),1,Q); % enlargement factor of apical membrane of
proximal tubule
198 kFKT = PeffK.*AK.*n;
199 kBLF = ((1./QBL) + 1./(PeffB.*AL)).^(-1);
200 kLFLT = PeffL.*AL;
201 kBGF = ((1./QBG) + 1./(PeffB.*AG)).^(-1);
202 kGFGT = PeffG.*AG;
203 kGLGT = PeffG.*AGL;
204 kBMF = ((1./QBM) + 1./(PeffB.*AM)).^(-1);
205 kMFMT = PeffM.*AM;
206 kBAF = ((1./QBA) + 1./(PeffB.*AA)).^(-1);
207 kAFAT = PeffA.*AA;
208 kBRF = ((1./QBR) + 1./(PeffB.*AR)).^(-1);
209 kRFRT = PeffR.*AR;
210 kbileLT = PeffL.*AL;
211
212 % First-order rate constants (s^-1).
213 bBKF = kBKF./(VB+VLB+VKB+VGB+VMB+VAB+VRB);
214 bKFB = kBKF./VKF;
215 bKFKT = kKFKT./VKF;
```

```
bKTKF = kKFKT./VKT;
bFKT = kFKT./VFil;
bKTF = kFKT./(VKT.*CRssK);
bBF = QGFR./(VB+VLB+VKB+VGB+VMB+VAB+VRB);
bFB = kBF./VFil;
bBLF = kBLF./(VB+VLB+VKB+VGB+VMB+VAB+VRB);
bLFB = kBLF./VLF;
bLFLT = kLFLT./VLF;
bLTLF = kLFLT./VLT;
bbileLT = kbileLT./Vbile;
bLTbile = kbileLT./(VLT.*CRssL);
bBGF = kBGF./(VB+VLB+VKB+VGB+VMB+VAB+VRB);
bGFB = kBGF./VGF;
bGFGT = kGFGT./VGF;
bGTGF = kGFGT./VGT;
bGLGT = kGLGT./VGL;
bGTGL = kGLGT./(VGT.*CRssG);
bBMF = kBMF./(VB+VLB+VKB+VGB+VMB+VAB+VRB);
bMFB = kBMF./VMF;
bMFMT = kMFMT./VMF;
bMTMF = kMFMT./VMT;
bBAF = kBAF./(VB+VLB+VKB+VGB+VMB+VAB+VRB);
bAFB = kBAF./VAF;
bAFAT = kAFAT./VAF;
bATAF = kAFAT./VAT;
bBRF = kBRF./(VB+VLB+VKB+VGB+VMB+VAB+VRB);
bRFB = kBRF./VRF;
bRFRT = kRFRT./VRF;
bRTRF = kRFRT./VRT;


% First-order rate constants (s^-1) for protein-mediated transport, see
% section S3-3 for details.
Pbclear = lognrnd(log(2.76e-7),0.5*log(5),1,Q);
bclear = Pbclear.*AK./VKF;
Pbreab = lognrnd(log(1.18e-7),0.5*log(5),1,Q);
breab = n.*Pbreab.*AK./VFil;
Pbabs = lognrnd(log(1.78e-7),0.5*log(5),1,Q);
babs = Pbabs.*AL./VLF;
Pbefflux = lognrnd(log(1.38e-7),0.5*log(5),1,Q);
befflux = Pbefflux.*AK./VKT;


% Conversion between mass and concentration for protein content of tissues.
MalbB = CalbB.*(VB+VLB+VKB+VGB+VMB+VAB+VRB);
MalbKF = CalbKF.*VKF;
ML_fabpKT1 = CL_fabpKT1.*VKT;
ML_fabpKT2 = CL_fabpKT2.*VKT;
ML_fabpKT3 = CL_fabpKT3.*VKT;
MK_fabpKT = Ca2uKT.*VKT;
MalbLF = CalbLF.*VLF;
ML_fabpLT1 = CL_fabpLT1.*VLT;
ML_fabpLT2 = CL_fabpLT2.*VLT;
ML_fabpLT3 = CL_fabpLT3.*VLT;
```

```
MalbGF = CalbGF.*VGF;
MalbMF = CalbMF.*VMF;
MalbAF = CalbAF.*VAF;
MalbRF = CalbRF.*VRF;


% Below is the numerical method used to solve mass balance equations.
seconds = 22*24*3600; % simulation time, 22 days
h = 0.07; % step size
tspan = (1:h:seconds);
steps = seconds./h;

% Initial condition for each comparment.
% Mass of PFOA in blood not bound to proteins: y1
% Mass of PFOA in blood bound to albumin: y2
% Mass of PFOA in interstitial fluid of kidney not bound to proteins: y3
% Mass of PFOA in interstitial fluid of kidney bound to albumin: y4
% Mass of PFOA in kidney tissue not bound to proteins: y5
% Mass of PFOA in kidney tissue bound to LFABP: y6, y61, and y62 (LFABP
% has 3 binding sites)
% Mass of PFOA in kidney tissue bound to alpha2mu-globulin: y7
% Mass of PFOA in renal filtrate not bound to proteins: y8
% Mass of PFOA in interstitial fluid of liver not bound to proteins: y9
% Mass of PFOA in interstitial fluid of liver bound to albumin: y10
% Mass of PFOA in liver tissue not bound to proteins: y11
% Mass of PFOA in liver tissue bound to LFABP: y12, y121, and y122 (LFABP
% has 3 binding sites)
% Mass of PFOA in bile not bound to proteins: y13
% Mass of PFOA in interstitial fluid of gut not bound to proteins: y14
% Mass of PFOA in interstitial fluid of gut bound to albumin: y15
% Mass of PFOA in gut tissue not bound to proteins: y16
% Mass of PFOA in interstitial fluid of muscle not bound to proteins: y17
% Mass of PFOA in interstitial fluid of muscle bound to albumin: y18
% Mass of PFOA in muscle tissue not bound to proteins: y19
% Mass of PFOA in interstitial fluid of adipose not bound to proteins: y20
% Mass of PFOA in interstitial fluid of adipose bound to albumin: y21
% Mass of PFOA in adipose tissue not bound to proteins: y22
% Mass of PFOA in interstitial fluid of the rest of body not bound to proteins
y23
% Mass of PFOA in interstitial fluid of the rest of body bound to albumin: y24
% Mass of PFOA in tissue of the rest of body not bound to proteins: y25
% Mass of PFOA in gut lumen not bound to proteins: y26
y1 = Dose.*BW.*ones([1,Q]);
y2 = zeros([1,Q]);
y3 = zeros([1,Q]);
y4 = zeros([1,Q]);
y5 = zeros([1,Q]);
y6 = zeros([1,Q]);
y61 = zeros([1,Q]);
y62 = zeros([1,Q]);
y7 = zeros([1,Q]);
y8 = zeros([1,Q]);
y9 = zeros([1,Q]);
y10 = zeros([1,Q]);
```

```
y11 = zeros([1,Q]);
y12 = zeros([1,Q]);
y121 = zeros([1,Q]);
y122 = zeros([1,Q]);
y13 = zeros([1,Q]);
y14 = zeros([1,Q]);
y15 = zeros([1,Q]);
y16 = zeros([1,Q]);
y17 = zeros([1,Q]);
y18 = zeros([1,Q]);
y19 = zeros([1,Q]);
y20 = zeros([1,Q]);
y21 = zeros([1,Q]);
y22 = zeros([1,Q]);
y23 = zeros([1,Q]);
y24 = zeros([1,Q]);
y25 = zeros([1,Q]);
y26 = zeros([1,Q]);

for j = 1:steps
    % Mass balance for available protein binding sites.
    MalbB_new = MalbB+h.*(koff.*y2-kon.*MalbB.*y1./(VB+VLB+VKB+VGB+VMB+VAB+VRB));
    MalbB = MalbB_new;
    CalbB = MalbB./(VB+VLB+VKB+VGB+VMB+VAB+VRB);
    MalbKF_new = MalbKF+h.*(koff.*y4-kon.*MalbKF.*y3./VKF);
    MalbKF = MalbKF_new;
    CalbKF = MalbKF./VKF;
    ML_fabpKT1_new = ML_fabpKT1+h.*(koff.*y6-kL_fabpon1.*ML_fabpKT1.*y5./VKT);
    ML_fabpKT1 = ML_fabpKT1_new;
    CL_fabpKT1 = ML_fabpKT1./VKT;
    ML_fabpKT2_new = ML_fabpKT2+h.*(koff.*y61-kL_fabpon2.*ML_fabpKT2.*y5./VKT);
    ML_fabpKT2 = ML_fabpKT2_new;
    CL_fabpKT2 = ML_fabpKT2./VKT;
    ML_fabpKT3_new = ML_fabpKT3+h.*(koff.*y62-kL_fabpon3.*ML_fabpKT3.*y5./VKT);
    ML_fabpKT3 = ML_fabpKT3_new;
    CL_fabpKT3 = ML_fabpKT3./VKT;
    MK_fabpKT_new = MK_fabpKT+h.*(koff.*y7-kK_fabpon.*MK_fabpKT.*y5./VKT);
    MK_fabpKT = MK_fabpKT_new;
    Ca2uKT = MK_fabpKT./VKT;
    MalbLF_new = MalbLF+h.*(koff.*y10-kon.*MalbLF.*y9./VLF);
    MalbLF = MalbLF_new;
    CalbLF = MalbLF./VLF;
    ML_fabpLT1_new = ML_fabpLT1 + h.*(koff.*y12 - kL_fabpon1.*ML_fabpLT1.*y11↙
/VLT);
    ML_fabpLT1 = ML_fabpLT1_new;
    CL_fabpLT1 = ML_fabpLT1./VLT;
    ML_fabpLT2_new = ML_fabpLT2+h.*(koff.*y121-kL_fabpon2.*ML_fabpLT2.*y11./VLT);
    ML_fabpLT2 = ML_fabpLT2_new;
    CL_fabpLT2 = ML_fabpLT2./VLT;
    ML_fabpLT3_new = ML_fabpLT3+h.*(koff.*y122-kL_fabpon3.*ML_fabpLT3.*y11./VLT);
    ML_fabpLT3 = ML_fabpLT3_new;
    CL_fabpLT3 = ML_fabpLT3./VLT;
    MalbGF_new = MalbGF+h.*(koff.*y15-kon.*MalbGF.*y14./VGF);
    MalbGF = MalbGF_new;
```

```
    CalbGF = MalbGF./VGF;
    MalbMF_new = MalbMF+h.*(koff.*y18-kon.*MalbMF.*y17./VMF);
    MalbMF = MalbMF_new;
    CalbMF = MalbMF./VMF;
    MalbAF_new = MalbAF+h.*(koff.*y21-kon.*MalbAF.*y20./VAF);
    MalbAF = MalbAF_new;
    CalbAF = MalbAF./VAF;
    MalbRF_new = MalbRF+h.*(koff.*y24-kon.*MalbRF.*y23./VRF);
    MalbRF = MalbRF_new;
    CalbRF = MalbRF./VRF;

    bBon = CalbB.*kon;
    bBoff = koff;
    bKFon = CalbKF.*kon;
    bKFoff = koff;
    bL_fabpKTon1 = CL_fabpKT1.*kL_fabpon1;
    bL_fabpKTon2 = CL_fabpKT2.*kL_fabpon2;
    bL_fabpKTon3 = CL_fabpKT3.*kL_fabpon3;
    bL_fabpKToff = koff;
    bK_fabpKTon = Ca2uKT.*kK_fabpon;
    bK_fabpKToff = koff;
    bLFon = CalbLF.*kon;
    bLFoff = koff;
    bL_fabpLTon1 = CL_fabpLT1.*kL_fabpon1;
    bL_fabpLTon2 = CL_fabpLT2.*kL_fabpon2;
    bL_fabpLTon3 = CL_fabpLT3.*kL_fabpon3;
    bL_fabpLToff = koff;
    bGFon = CalbGF.*kon;
    bGFoff = koff;
    bMFon = CalbMF.*kon;
    bMFoff = koff;
    bAFon = CalbAF.*kon;
    bAFoff = koff;
    bRFon = CalbRF.*kon;
    bRFoff = koff;

    % Differential mass balance for each tissue or fluid compartment.
    y1_new = y1 + h.*(bKFB.*y3+bLFB.*y9-bBLF.*y1-bBKF.*y1-bBon.*y1+bBoff.*y2-bBF↙
*y1+bFB.*y8+bGFB.*y14-bBGF.*y1+bMFB.*y17-bBMF.*y1+bAFB.*y20-bBAF.*y1+bRFB.*y23-bBRF↙
*y1);
    y1 = max(y1_new,0);
    y2_new = y2 + h.*(bBon.*y1-bBoff.*y2);
    y2 = max(y2_new,0);
    y3_new = y3 + h.*(bBKF.*y1-bKFB.*y3+befflux.*y5+bKTKF.*y5-bKFKT.*y3-bclear↙
*y3+bKFoff.*y4-bKFon.*y3);
    y3 = max(y3_new,0);
    y4_new = y4 + h.*(bKFon.*y3-bKFoff.*y4);
    y4 = max(y4_new,0);
    y5_new = y5 + h.*(bKFKT.*y3+bFKT.*y8+breab.*y8+bclear.*y3-befflux.*y5-bKTKF↙
*y5-bKTF.*y5+bL_fabpKToff.*y6-bL_fabpKTon1.*y5+bL_fabpKToff.*y61-bL_fabpKTon2↙
*y5+bL_fabpKToff.*y62-bL_fabpKTon3.*y5+bK_fabpKToff.*y7-bK_fabpKTon.*y5);
    y5 = max(y5_new,0);
    y6_new = y6 + h.*(bL_fabpKTon1.*y5-bL_fabpKToff.*y6);
    y6 = max(y6_new,0);
```

```
425     y61_new = y61 + h.*(bL_fabpKTon2.*y5-bL_fabpKToff.*y61);
426     y61 = max(y61_new,0);
427     y62_new = y62 + h.*(bL_fabpKTon3.*y5-bL_fabpKToff.*y62);
428     y62 = max(y62_new,0);
429     y7_new = y7 + h.*(bK_fabpKTon.*y5-bK_fabpKToff.*y7);
430     y7 = max(y7_new,0);
431     y8_new = y8 + h.*(bKTF.*y5-breab.*y8+bBF.*y1-bFB.*y8-bFKT.*y8-Qurine.*y8↙
/VFil);
432     y8 = max(y8_new,0);
433     y9_new = y9 + h.*(bBLF.*y1-bLFB.*y9+bLTLF.*y11-bLFLT.*y9-babs.*y9-bLFon↙
*y9+bLFoff.*y10);
434     y9 = max(y9_new,0);
435     y10_new = y10 + h.*(bLFon.*y9-bLFoff.*y10);
436     y10 = max(y10_new,0);
437     y11_new = y11 + h.*(bLFLT.*y9+babs.*y9+bbileLT.*y13-bLTbile.*y11-bLTLF.*y11↙
bL_fabpLTon1.*y11+bL_fabpLToff.*y12-bL_fabpLTon2.*y11+bL_fabpLToff.*y121↙
bL_fabpLTon3.*y11+bL_fabpLToff.*y122);
438     y11 = max(y11_new,0);
439     y12_new = y12 + h.*(bL_fabpLTon1.*y11-bL_fabpLToff.*y12);
440     y12 = max(y12_new,0);
441     y121_new = y121 + h.*(bL_fabpLTon2.*y11-bL_fabpLToff.*y121);
442     y121 = max(y121_new,0);
443     y122_new = y122 + h.*(bL_fabpLTon3.*y11-bL_fabpLToff.*y122);
444     y122 = max(y122_new,0);
445     y13_new = y13 + h.*(bLTbile.*y11-bbileLT.*y13-Qbile.*y13./Vbile);
446     y13 = max(y13_new,0);
447     y14_new = y14 + h.*(bBGF.*y1-bGFB.*y14+bGTGF.*y16-bGFGT.*y14-bGFon↙
*y14+bGFoff.*y15);
448     y14 = max(y14_new,0);
449     y15_new = y15 + h.*(bGFon.*y14-bGFoff.*y15);
450     y15 = max(y15_new,0);
451     y16_new = y16 + h.*(bGFGT.*y14-bGTGF.*y16+bGLGT.*y26-bGTGL.*y16);
452     y16 = max(y16_new,0);
453     y17_new = y17 + h.*(bBMF.*y1-bMFB.*y17+bMTMF.*y19-bMFMT.*y17-bMFon↙
*y17+bMFoff.*y18);
454     y17 = max(y17_new,0);
455     y18_new = y18 + h.*(bMFon.*y17-bMFoff.*y18);
456     y18 = max(y18_new,0);
457     y19_new = y19 + h.*(bMFMT.*y17-bMTMF.*y19);
458     y19 = max(y19_new,0);
459     y20_new = y20 + h.*(bBAF.*y1-bAFB.*y20+bATAF.*y22-bAFAT.*y20-bAFon↙
*y20+bAFoff.*y21);
460     y20 = max(y20_new,0);
461     y21_new = y21 + h.*(bAFon.*y20-bAFoff.*y21);
462     y21 = max(y21_new,0);
463     y22_new = y22 + h.*(bAFAT.*y20-bATAF.*y22);
464     y22 = max(y22_new,0);
465     y23_new = y23 + h.*(bBRF.*y1-bRFB.*y23+bRTRF.*y25-bRFRT.*y23-bRFon↙
*y23+bRFoff.*y24);
466     y23 = max(y23_new,0);
467     y24_new = y24 + h.*(bRFon.*y23-bRFoff.*y24);
468     y24 = max(y24_new,0);
469     y25_new = y25 + h.*(bRFRT.*y23-bRTRF.*y25);
470     y25 = max(y25_new,0);
```

```
    y26_new = y26 + h.*(bGTGL.*y16-bGLGT.*y26+Qbile.*y13./Vbile-Qfeces.*y26↙
/VGL);
    y26 = max(y26_new,0);

    yBfree = y1;
    yBbound = y2;
    yKFfree = y3;
    yKFbound = y4;
    yKTfree = y5;
    yKTLbound1 = y6;
    yKTLbound2 = y61;
    yKTLbound3 = y62;
    yKTKbound = y7;
    yFfree = y8;
    yLFfree = y9;
    yLFbound = y10;
    yLTfree = y11;
    yLTbound1 = y12;
    yLTbound2 = y121;
    yLTbound3 = y122;
    yBile = y13;
    yGFfree = y14;
    yGFbound = y15;
    yGTfree = y16;
    yMFfree = y17;
    yMFbound = y18;
    yMTfree = y19;
    yAFfree = y20;
    yAFbound = y21;
    yATfree = y22;
    yRFfree = y23;
    yRFbound = y24;
    yRTfree = y25;
    yGLfree = y26;

    i = round(1 + j./3600)
    t(i,:) = j*h./(24*3600);

    % Unit conversion from kg/m^3 to ng/g.
    Blood(i,:) = (yBfree+yBbound)./(VB+VLB+VKB+VGB+VMB+VAB+VRB).*VB./Vplasma↙
*10^6;
    Kidney(i,:) = ((yBfree+yBbound)./(VB+VLB+VKB+VGB+VMB+VAB+VRB)↙
*VKB+yKFfree+yKFbound+yKTfree+yKTLbound1+yKTLbound2+yKTLbound3+yKTKbound).↙
(VKB+VKT+VKF).*10^6;
    Liver(i,:) = ((yBfree+yBbound)./(VB+VLB+VKB+VGB+VMB+VAB+VRB)↙
*VLB+yLFfree+yLFbound+yLTfree+yLTbound1+yLTbound2+yLTbound3)./(VLB+VLT+VLF).*10^6;
    Gut(i,:) = ((yBfree+yBbound)./(VB+VLB+VKB+VGB+VMB+VAB+VRB)↙
*VGB+yGFfree+yGFbound+yGTfree)./(VGB+VGT+VGF).*10^6;
    Muscle(i,:) = ((yBfree+yBbound)./(VB+VLB+VKB+VGB+VMB+VAB+VRB)↙
*VMB+yMFfree+yMFbound+yMTfree)./(VMB+VMT+VMF).*10^6;
    Adipose(i,:) = ((yBfree+yBbound)./(VB+VLB+VKB+VGB+VMB+VAB+VRB)↙
*VAB+yAFfree+yAFbound+yATfree)./(VAB+VAT+VAF).*10^6;
    Rest(i,:) = ((yBfree+yBbound)./(VB+VLB+VKB+VGB+VMB+VAB+VRB)↙
*VRB+yRFfree+yRFbound+yRTfree)./(VRB+VRT+VRF).*10^6;
```

```
    Feces(i,:) = yGLfree./VGL.*10^6;
    Bile(i,:) = yBile./Vbile.*10^6;
    Urine(i,:) = yFfree./VFil.*10^6;

end


% Sensitivity analysis using Pearson ranked correlation between sampled
% parameters and predicted PFOA concentrations, shown here for blood,
% sampled on Day 12.
rho1 = corr((Blood(4115,:))',[BW',Dose',PVB',PVplasma',PVK',PVKB',...
    PVKF',VFil',PVL',PVLB',PVLF',PVbile',PVG',PVGB',PVGF',PVGL',...
    PVM',PVMB',PVMF',PVA',PVAB',PVAF',PVRB',PVRF',PQBK',...
    PQGFR',PQurine',PQBL',PQbile',Qfeces',PQBG',PQBM',PQBA',...
    PAK',n',PAKG',PAL',PAG',PAGL',PAM',PAA',PAR',PeffB',PeffK',...
    PeffL',PeffG',PeffM',PeffA',PeffR',CRssG',CRssL',CRssK',...
    CalbB',CalbKF',CL_fabpKT',Ca2uKT',CalbLF',CL_fabpLT',CalbGF',...
    CalbMF',CalbAF',CalbRF',Ka',KL_fabp1',KL_fabp2',KL_fabp3',Ka2u',...
    koff',Pbclear',Pbreab',Pbefflux',Pbabs']);
```

References

(1) Davies, B.; Morris, T. Physiological parameters in laboratory animals and humans. *Pharm. Res.* **1993,** *10* (7), 1093-1095.

(2) Brown, R. P.; Delp, M. D.; Lindstedt, S. L.; Rhomberg, L. R.; Beliles, R. P. Physiological parameter values for physiologically based pharmacokinetic models. *Toxicol. Ind. Health* **1997,** *13* (4), 407-484.

(3) Blouin, A.; Bolender, R. P.; Weibel, E. R. Distribution of organelles and membranes between hepatocytes and nonhepatocytes in the rat liver parenchyma. A stereological study. *J. Cell Biol.* **1977,** *72* (2), 441-455.

(4) Larson, M.; Sjöquist, M.; Wolgast, M. Renal interstitial volume of the rat kidney. *Acta Physiol. Scand.* **1984,** *120* (2), 297-304.

(5) Barratt, T. M.; Walser, M. Extracellular fluid in individual tissues and in whole animals: the distribution of radiosulfate and radiobromide. *J. Clin. Invest.* **1969,** *48* (1), 56.

(6) Ng, C. A.; Hungerbühler, K. Bioconcentration of perfluorinated alkyl acids: how important is specific binding? *Environ. Sci. Technol.* **2013,** *47* (13), 7214-7223.

(7) Everett, N. B.; Simmons, B.; Lasher, E. P. Distribution of blood (Fe59) and plasma (I131) volumes of rats determined by liquid nitrogen freezing. *Circul. Res.* **1956,** *4*, 419-424.

(8) Crone, C. The permeability of capillaries in various organs as determined by use of the 'indicator diffusion'method. *Acta Physiol. Scand.* **1963,** *58* (4), 292-305.

(9) McConnell, E. L.; Basit, A. W.; Murdan, S. Measurements of rat and mouse gastrointestinal pH, fluid and lymphoid tissue, and implications for in‐vivo experiments. *J. Pharm. Pharmacol.* **2008,** *60* (1), 63-70.

(10) Munger, K.; Baylis, C. Sex differences in renal hemodynamics in rats. *Am. J. Physiol. Renal Physiol.* **1988,** *254* (2), F223-F231.

(11) Biewald, N.; Billmeier, J. Blood volume and extracellular space (ECS) of the whole body and some organs of the rat. *Experientia* **1978,** *34* (3), 412-413.

(12) Kirkman, H.; Stowell, R. Renal filtration surface in the albino rat. *Anat. Rec.* **1942,** *82* (3), 373-391.

(13) DeSesso, J.; Jacobson, C. Anatomical and physiological parameters affecting gastrointestinal absorption in humans and rats. *Food Chem. Toxicol.* **2001,** *39* (3), 209-228.

(14) Arthur, S.; Green, R. Fluid reabsorption by the proximal convoluted tubule of the kidney in lactating

rats. *J. Physiol.* **1986,** *371*, 267.

(15) Bonvalet, J.; de Rouffignac, C. Distribution of ferrocyanide along the proximal tubular lumen of the rat kidney: its implications upon hydrodynamics. *J. Physiol.* **1981,** *318*, 85.

(16) Frazier, K. S.; Seely, J. C.; Hard, G. C.; Betton, G.; Burnett, R.; Nakatsuji, S.; Nishikawa, A.; Durchfeld-Meyer, B.; Bube, A. Proliferative and nonproliferative lesions of the rat and mouse urinary system. *Toxicol. Pathol.* **2012,** *40* (4 suppl), 14S-86S.

(17) Kanauchi, O.; Agata, K.; Fushiki, T. Mechanism for the increased defecation and jejunum mucosal protein content in rats by feeding germinated barley foodstuff. *Biosci., Biotechnol., Biochem.* **1997,** *61* (3), 443-448.

(18) Cavigelli, S.; Monfort, S.; Whitney, T.; Mechref, Y.; Novotny, M.; McClintock, M. Frequent serial fecal corticoid measures from rats reflect circadian and ovarian corticosterone rhythms. *J. Endocrinol.* **2005,** *184* (1), 153-163.

(19) Crisman, T. S.; Claffey, K. P.; Saouaf, R.; Hanspal, J.; Brecher, P. Measurement of rat heart fatty acid binding protein by ELISA. Tissue distribution, developmental changes and subcellular distribution. *J. Mol. Cell. Cardiol.* **1987,** *19* (5), 423-431.

(20) Levitt, D. G. The pharmacokinetics of the interstitial space in humans. *BMC Clin. Pharmacol.* **2003,** *3* (1), 3.

(21) Ockner, R. K.; Manning, J.; Kane, J. Fatty acid binding protein. Isolation from rat liver, characterization, and immunochemical quantification. *J. Biol. Chem.* **1982,** *257* (13), 7872-7878.

(22) Maatman, R. G.; van de Westerlo, E. M.; Van Kuppevelt, T.; Veerkamp, J. H. Molecular identification of the liver-and the heart-type fatty acid-binding proteins in human and rat kidney. Use of the reverse transcriptase polymerase chain reaction. *Biochem. J.* **1992,** *288* (1), 285-290.

(23) Kimura, H.; Odani, S.; Nishi, S.; Sato, H.; Arakawa, M.; Ono, T. Primary structure and cellular distribution of two fatty acid-binding proteins in adult rat kidneys. *J. Biol. Chem.* **1991,** *266* (9), 5963-5972.

(24) Ellmerer, M.; Schaupp, L.; Brunner, G. A.; Sendlhofer, G.; Wutte, A.; Wach, P.; Pieber, T. R. Measurement of interstitial albumin in human skeletal muscle and adipose tissue by open-flow microperfusion. *Am. J. Physiol. Endocrinol. Metab.* **2000,** *278* (2), E352-E356.

(25) Peters, T. The biosynthesis of rat serum albumin II. Intracellular phenomena in the secretion of newly

formed albumin. *J. Biol. Chem.* **1962,** *237* (4), 1186-1189.

(26) Han, X.; Snow, T. A.; Kemper, R. A.; Jepson, G. W. Binding of perfluorooctanoic acid to rat and human plasma proteins. *Chem. Res. Toxicol.* **2003,** *16* (6), 775-781.

(27) Woodcroft, M. W.; Ellis, D. A.; Rafferty, S. P.; Burns, D. C.; March, R. E.; Stock, N. L.; Trumpour, K. S.; Yee, J.; Munro, K. Experimental characterization of the mechanism of perfluorocarboxylic acids' liver protein bioaccumulation: The key role of the neutral species. *Environ. Toxicol. Chem.* **2010,** *29* (8), 1669-1677.

(28) Han, X.; Hinderliter, P. M.; Snow, T. A.; Jepson, G. W. Binding of Perfluorooctanoic Acid to Rat Liver - form and Kidney - form α 2u - Globulins. *Drug Chem. Toxicol.* **2004,** *27* (4), 341-360.

(29) Weaver, Y. M.; Ehresman, D. J.; Butenhoff, J. L.; Hagenbuch, B. Roles of rat renal organic anion transporters in transporting perfluorinated carboxylates with different chain lengths. *Toxicol. Sci.* **2009**, kfp275.

(30) Zhao, W.; Zitzow, J. D.; Ehresman, D. J.; Chang, S.-C.; Butenhoff, J. L.; Forster, J.; Hagenbuch, B. Na+/taurocholate cotransporting polypeptide and apical sodium-dependent bile acid transporter are involved in the disposition of perfluoroalkyl sulfonates in humans and rats. *Toxicol. Sci.* **2015**, kfv102.

(31) Han, X.; Nabb, D. L.; Russell, M. H.; Kennedy, G. L.; Rickard, R. W. Renal elimination of perfluorocarboxylates (PFCAs). *Chem. Res. Toxicol.* **2011,** *25* (1), 35-46.

(32) Yang, C.-H.; Glover, K. P.; Han, X. Characterization of cellular uptake of perfluorooctanoate via organic anion-transporting polypeptide 1A2, organic anion transporter 4, and urate transporter 1 for their potential roles in mediating human renal reabsorption of perfluorocarboxylates. *Toxicol. Sci.* **2010,** *117* (2), 294-302.

(33) Kemper, R. A. Perfluorooctanoic acid: toxicokinetics in the rat. *Project ID: DuPont* **2003,** *7473*.

(34) MacLeod, M.; Fraser, A. J.; Mackay, D. Evaluating and expressing the propagation of uncertainty in chemical fate and bioaccumulation models. *Environ. Toxicol. Chem.* **2002,** *21* (4), 700-709.

(35) Hebert, P. C.; MacManus-Spencer, L. A. Development of a fluorescence model for the binding of medium-to long-chain perfluoroalkyl acids to human serum albumin through a mechanistic evaluation of spectroscopic evidence. *Anal. Chem.* **2010,** *82* (15), 6463-6471.

(36) Yang, Y.; Xu, X.; Georgopoulos, P. G. A Bayesian population PBPK model for multiroute chloroform exposure. *J. Expo. Sci. Environ. Epidemiol.* **2010,** *20* (4), 326-341.

(37) Kim, S.-J.; Heo, S.-H.; Lee, D.-S.; Hwang, I. G.; Lee, Y.-B.; Cho, H.-Y. Gender differences in pharmacokinetics and tissue distribution of 3 perfluoroalkyl and polyfluoroalkyl substances in rats. *Food Chem. Toxicol.* **2016,** *97*, 243-255.

(38) Kudo, N.; Sakai, A.; Mitsumoto, A.; Hibino, Y.; Tsuda, T.; Kawashima, Y. Tissue distribution and hepatic subcellular distribution of perfluorooctanoic acid at low dose are different from those at high dose in rats. *Biol. Pharm. Bull.* **2007,** *30* (8), 1535-1540.